

Chapter 5

Collective Dynamics and Synchronization in Small Assemblies of Neural Pairs

The unique capabilities of the brain to perform cognitive tasks are an outcome of the collective global behavior of its constituent neurons. This is the motivation for investigating the dynamics of small networks of excitatory-inhibitory neural pairs, which have been studied in isolation so far. Recent neurobiological studies have shown that many cortical neurons respond to behavioral events with rapid modulations of discharge correlations, lasting between $\sim 10^{-2} - 10$ seconds [193]. This supports the notion that a neuron can intermittently participate in different computations by rapid synchronization and desynchronization with neighboring neurons. The mechanism of such dynamic correlations in the brain are as yet unknown.

Observation of transition between synchronized activity and incoherent activity in the brain during sensory perception [53], hints at a connection with phase-locking among coupled chaotic systems. Under certain conditions, such chaotic systems can synchronize, either through coupling, or by being linked to a common signal. However, the presence of multiple synchronizing interactions in a network of chaotic elements shows a variety of novel phenomena. The numerical observations reported in this chapter provide a glimpse of the possible range of collective behavior in small assemblies of chaotic neural pairs. Section 1 reviews some techniques for synchronizing chaotic systems. In Section 2 we briefly mention several interesting features observed during the synchronization of two or three coupled neural pairs (both unidirectional and bidirectional couplings have been considered). Section 3 introduces the model (based on the Lorenz system of equations) used for studying competition among synchronizing chaotic systems and includes a short analysis of the fixed points and their stability. Section 4 contains the results of computer simulations of the system. Finally, possible directions of future research and the relevance of this type of research to the theory of neural computation are discussed.

5.1 Synchronization of chaotic systems

The synchronization of chaotic systems is a difficult problem owing to their extremely sensitive dependence on initial conditions. Any initial correlation present between identical systems, starting from very close initial conditions, exponentially decrease to zero with time. Thus, for all practical purposes, any initial synchronization between the systems is bound to disappear rapidly. In recent times, however, some methods of achieving synchronized behavior between chaotic systems have been proposed. Pioneering work in this respect has been done by Pecora and Carroll [140], who used the concept of a response system locking on to a driver system. So far, such studies have been limited to driving a response system by a single driver system. However, the knowledge gained from studying such simple systems may not be adequate to give us an idea as to how systems consisting of multiple independent driver systems, competing with each other to synchronize the same response system, will behave. The Pecora-Carroll driving mechanism can be seen as the “strong-coupling” limit of a general scheme of directionally- oriented couplings in a network of chaotic elements.

The synchronization of bidirectionally coupled chaotic systems is stable provided the coupling strength is at least half the Lyapunov exponent of the system [55] (when the coupling includes all the components of the system equally). One-way coupling (or, driving one chaotic system by another) can also lead to synchronization, provided certain conditions are satisfied [140], [141], [81]. The drive-response method consist of the following steps. First an n -dimensional autonomous system

$$\frac{d\mathbf{x}}{dt} = \mathbf{F}(\mathbf{x}),$$

is divided into two parts, driving (\mathbf{x}_d) and responding (\mathbf{x}_r):

$$\frac{d\mathbf{x}_d}{dt} = \mathbf{g}(\mathbf{x}_d, \mathbf{x}_r), \quad \frac{d\mathbf{x}_r}{dt} = \mathbf{h}(\mathbf{x}_d, \mathbf{x}_r),$$

where, $\mathbf{x}_d = (x_1, \dots, x_m)$, $\mathbf{g} = [f_1(\mathbf{x}), \dots, f_m(\mathbf{x})]$, $\mathbf{x}_r = (x_{m+1}, \dots, x_n)$ and $\mathbf{h} = [f_{m+1}(\mathbf{x}), \dots, f_n(\mathbf{x})]$. A replica subsystem \mathbf{x}'_r identical to \mathbf{x}_r is then created and driven with the \mathbf{x}_d variables of the original system. Therefore, the replica subsystem equations are,

$$\frac{d\mathbf{x}'_r}{dt} = \mathbf{h}(\mathbf{x}_d, \mathbf{x}'_r).$$

The responding subsystems \mathbf{x}_r and \mathbf{x}'_r will synchronize only if $\delta\mathbf{x}_r = |\mathbf{x}_r - \mathbf{x}'_r| \rightarrow 0$. According to Pecora and Carroll, this occurs if and only if the conditional Lyapunov exponents of the \mathbf{x}_r subsystem are all negative.

Drive-response synchronization has been realized in various electrical circuit experiments. It has also been used in experiments of secure communication where a chaotic masking signal is added to the transmitted signal. It is then recovered at the receiving end by subtracting the chaotic signal regenerated by synchronization [42].

Besides the Pecora-Carroll method, other synchronization procedures have also been proposed. Of these, the Variable Control Feedback (VCF) method is of particular interest, as it can be used for both control and synchronization of chaos [92]. In fact, the Pecora-Carroll method turns out to be a special limiting case of this method. VCF consists of adding a feedback term to a dynamical system to guide it into some prescribed state. If $\frac{dx}{dt} = F(x)$ be an n -dimensional dynamical system and x^* be the desired state to which the system has to be brought, then VCF involves modifying the system dynamics to:

$$\frac{dx}{dt} = F(x) - \lambda(x - x^*)$$

where λ is the set of n feedback multipliers. If x^* be the output of a chaotic system $F'(x)$, then the system synchronizes with $F(x)$. In the large- λ limit, VCF reduces to the Pecora-Carroll method. Specifically, the feedback parameters for the driving subsystem variables, $\lambda_d \rightarrow \infty$, while the remaining λ s are set to zero.

5.2 Collective dynamics of neural assemblies

Synchronization among chaotic maps, with either unidirectional or bidirectional coupling, have been investigated previously in [46, 78, 189], while the effect of coupling on the chaotic dynamics has been studied in [115, 152, 63, 143]. In this section we briefly mention some results of numerical investigations of collective dynamics of N pairs of excitatory-inhibitory neural pairs ($N=2,3$), coupled to each other, either unidirectionally or bidirectionally. The cases considered are shown schematically in Fig. 5.1.

Case I: $N = 2$

In this case, synchronization occurs for both unidirectional and bidirectional coupling, when the magnitude of the coupling parameter is above a certain critical threshold. An interesting feature observed is the intermittent occurrence of desynchronization [56, 82] in an apparently synchronized situation, for a range of coupling values. The arrangements we have investigated numerically are given by the following set of equations:

$$\begin{aligned} z_{n+1}^1 &= IF(z_n^1), \\ z_{n+1}^2 &= IF(z_n^2 + \lambda[z_n^1 - z_n^2]), \end{aligned}$$

for unidirectional coupling, and

$$\begin{aligned} z_{n+1}^1 &= IF(z_n^1 + \lambda[z_n^2 - z_n^1]), \\ z_{n+1}^2 &= IF(z_n^2 + \lambda[z_n^1 - z_n^2]), \end{aligned}$$

for bidirectional coupling (IF indicates the dynamical system representing an excitatory-inhibitory neural pair, with sigmoid activation function). Both systems show qualitatively similar behavior. In Fig. 5.2, we present the results of numerical simulation


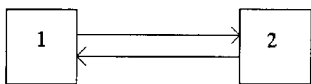
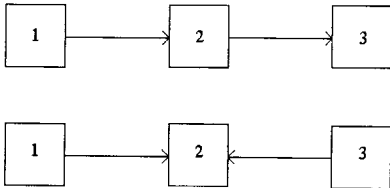
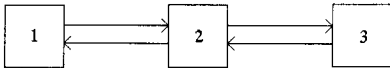
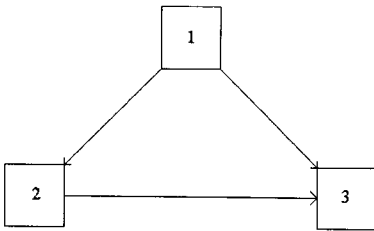
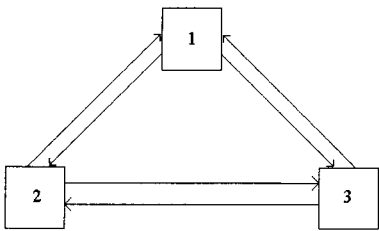
		Unidirectional Coupling	Bidirectional Coupling
N = 2		 <p>(a)</p>	 <p>(b)</p>
N = 3	LOCAL	 <p>(c)</p>	 <p>(d)</p>
	GLOBAL	 <p>(e)</p>	 <p>(f)</p>

Figure 5.1: The coupling arrangements investigated for $N = 2$ ((a) unidirectional and (b) bidirectional) and $N = 3$ neural pairs. In the latter case, two further cases were considered: local coupling ((c) unidirectional and (d) bidirectional) and global coupling ((e) unidirectional and (f) bidirectional).

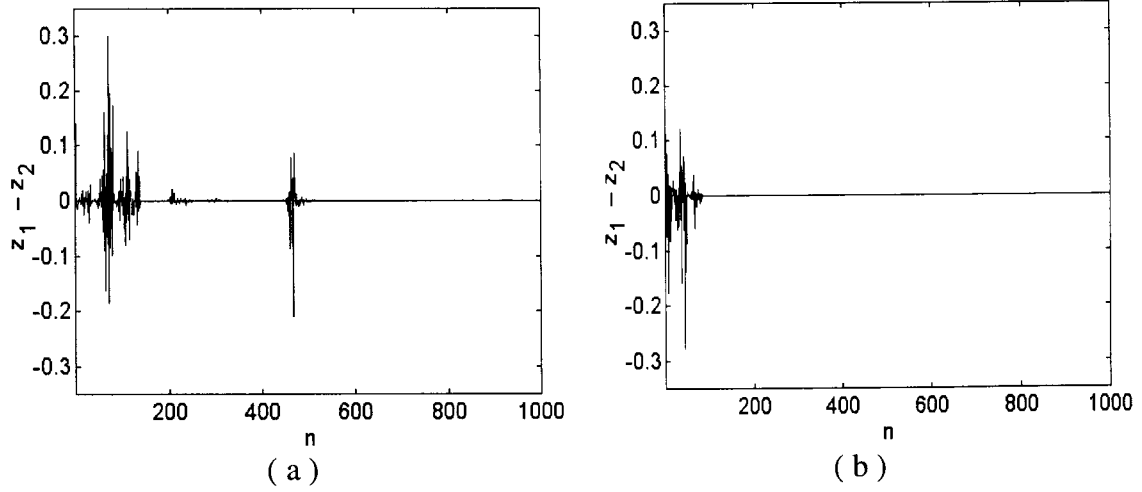


Figure 5.2: Intermittent synchronization for 2 bidirectionally coupled neural pairs (z_1, z_2) with coupling magnitude (a) $\lambda = 0.26$ and (b) $\lambda = 0.28$ ($a = 100, b = 25$, for both the pairs).

of a bidirectionally coupled system, where the component neural pairs have the activation function parameters $a = 100, b = 25$. As can be seen clearly, the presence of intermittent burst of desynchronization occurs as a function of the coupling parameter, λ .

Case II: $N = 3$

For $N = 3$, two coupling arrangements are possible for both unidirectional and bidirectional coupling: *local coupling*, where nearest neighbors are coupled to each other, and *global coupling*, where the elements are coupled in an all-to-all fashion.

In the case of unidirectional coupling, a certain type of local coupling arrangement can produce a situation, referred to as “frustrated synchronization”, that has been analysed in detail later in this chapter. In the case of bidirectional coupling, we observe a new phenomenon, referred to as *mediated synchronization*. The equations governing the dynamics of the coupled system is given by:

$$\begin{aligned} z_{n+1}^1 &= \mathcal{F}(z_n^1 + \lambda z_n^2), \\ z_{n+1}^2 &= \mathcal{F}(z_n^2 + \lambda[z_n^1 + z_n^3]), \\ z_{n+1}^3 &= \mathcal{F}(z_n^3 + \lambda z_n^2). \end{aligned}$$

For the set of activation parameters $a = 100, b = 25$, we observe the following feature over a range of values of the coupling parameter, λ : the neural pairs, z^1 and z^3 which have no direct connection between themselves synchronize, although z^2

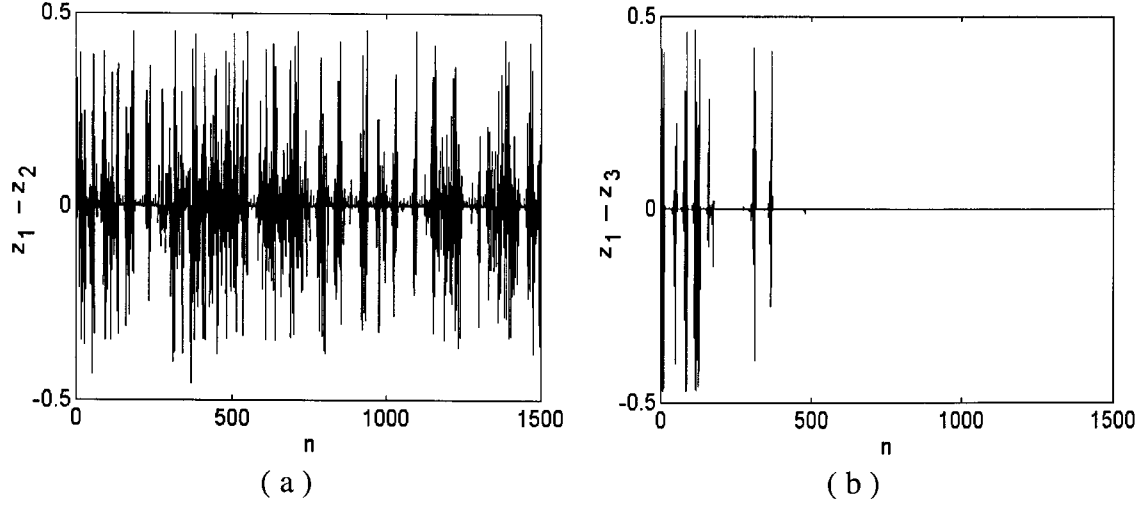


Figure 5.3: Mediated synchronization for 3 bidirectional, locally coupled neural pairs (z_1, z_2, z_3) with coupling magnitude $\lambda = 0.12$: (a) no synchronization between z_1 and z_2 , while, (b) z_1 and z_3 synchronize after ~ 500 iterations ($a = 100, b = 25$ for all the pairs).

synchronizes with neither (Fig. 5.3). So, the system z^2 appears to be “mediating” the synchronization interaction, although not taking part in it by itself.

For a global coupling arrangement, no new feature is observed for unidirectional coupling (this arrangement is similar to that studied in [13] for continuous time systems) - but for bidirectional coupling, governed by the set of equations:

$$\begin{aligned} z_{n+1}^1 &= \mathcal{IF}(z_n^1 + \lambda[z_n^2 + z_n^3]), \\ z_{n+1}^2 &= \mathcal{IF}(z_n^2 + \lambda[z_n^1 + z_n^3]), \\ z_{n+1}^3 &= \mathcal{IF}(z_n^3 + \lambda[z_n^1 + z_n^2]), \end{aligned}$$

the phenomenon of “frustrated synchronization” is observed. The phase space of the entire coupled system is shown in Fig. 5.4. The time series plots in Fig 5.5 show that none of the component systems synchronize. This is because the 3 systems, each trying to synchronize the other, frustrate all attempts at collective synchronization. (Note that the introduction of structural disorder in chaotic systems can also lead to frustration [26].) To study this phenomenon in detail in the unidirectionally coupled situation, we have considered the well-known Lorenz system of equations in the following section.

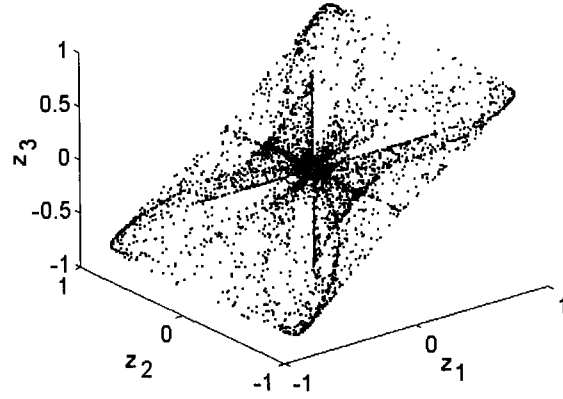


Figure 5.4: Phase space for 3 bidirectional, globally coupled neural pairs (z_1, z_2, z_3) with coupling magnitude $\lambda = 0.5$ ($a = 100, b = 5$ for all the pairs).

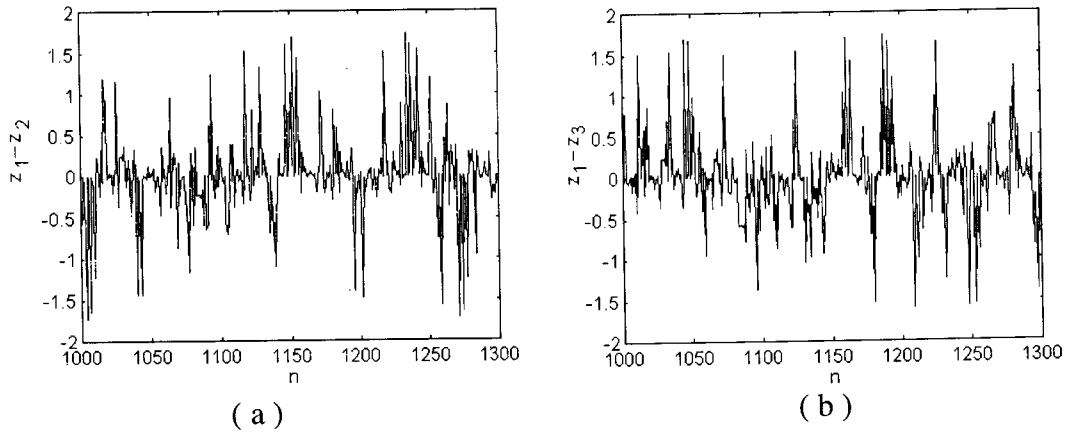


Figure 5.5: Frustrated synchronization for 3 bidirectional, globally coupled neural pairs (z_1, z_2, z_3) with coupling magnitude $\lambda = 0.5$: no synchronization between (a) z_1 and z_2 , or, (b) z_1 and z_3 ($a = 100, b = 5$ for all the pairs).

5.3 Competition among synchronizing Lorenz systems

The investigation of competition among synchronizing chaotic systems was carried out using the Lorenz system of equations [114], [182]. This well-known paradigm of chaos is defined by the following set of equations:

$$\frac{dx}{dt} = \sigma (y - x), \quad (5.1)$$

$$\frac{dy}{dt} = rx - y - xz, \quad (5.2)$$

$$\frac{dz}{dt} = xy - bz, \quad (5.3)$$

where, σ , r and b are real, positive parameters. There are three fixed points for this system: $F_1 = (0, 0, 0)$, $F_2 = (\sqrt{b(r-1)}, \sqrt{b(r-1)}, r-1)$, and $F_3 = (-\sqrt{b(r-1)}, -\sqrt{b(r-1)}, r-1)$. The local stability of the fixed point (x_f, y_f, z_f) is determined by the eigenvalues of the Jacobian

$$J = \begin{vmatrix} -\sigma & \sigma & 0 \\ (r - z_f) & -1 & -x_f \\ y_f & x_f & -b \end{vmatrix}. \quad (5.4)$$

Evaluation of the matrix shows that for $0 < r < 1$, F_1 is the only stable fixed point. For $r > 1$, F_1 becomes unstable and the phase-space trajectory of the system converges to either F_2 or F_3 . For $r > r_c = \sigma(\sigma + b + 3)/(\sigma - b - 1)$ the system's trajectory perpetually wanders along the extremely complicated structure of the stable and unstable manifolds of the fixed points, exhibiting chaotic behavior.

For the present work the effect of two driving systems, designated as driving systems 1 (x_1, y_1, z_1) and 2 (x_2, y_2, z_2) , competing to synchronize a responding system (x_3, y_3, z_3) was studied. The responding system was driven using the y variable. A competition parameter a was defined to indicate the strength of the driving systems relative to each other. The maximum value of a was normalized to unity. Therefore, the y variable of the responding system was defined in terms of the two driving systems as:

$$y_3 = ay_1 + (1 - a)y_2. \quad (5.5)$$

We consider first the case where the two driving systems have the same r -parameter value, and then, the more general case, where the two r -values are different (r_1 and r_2 , say). The σ and b -parameter values are considered to be the same in all cases.

Case I: $r_1 = r_2 = r$

It is obvious that for $a = 1$ the responding system synchronizes with driver system 1, whereas for $a = 0$, it synchronizes with system 2. The attractor of the response

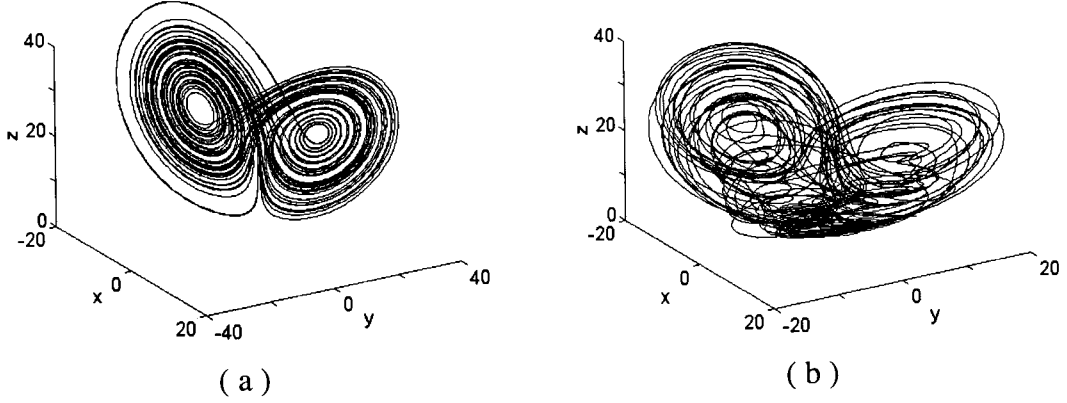


Figure 5.6: The response system attractor for (a) $a = 1.0$ and (b) $a = 0.5$ ($r_1 = r_2 = 28, \sigma = 10, b = 8/3$).

system, is identical to that of the conventional Lorenz system (Fig. 5.6 (a)). For $0 < a < 1$, the responding system (x_3, y_3, z_3) has nine fixed points:

$$\begin{aligned}
 F_1 &= (0, 0, 0), \\
 F_2 &= (\sqrt{b(r-1)}, \sqrt{b(r-1)}, r-1), \\
 F_3 &= (-\sqrt{b(r-1)}, -\sqrt{b(r-1)}, r-1), \\
 F_4 &= (a\sqrt{b(r-1)}, a\sqrt{b(r-1)}, a^2(r-1)), \\
 F_5 &= ((1-a)\sqrt{b(r-1)}, (1-a)\sqrt{b(r-1)}, (1-a)^2(r-1)), \\
 F_6 &= (-a\sqrt{b(r-1)}, -a\sqrt{b(r-1)}, a^2(r-1)), \\
 F_7 &= (-(1-a)\sqrt{b(r-1)}, -(1-a)\sqrt{b(r-1)}, (1-a)^2(r-1)), \\
 F_8 &= ((2a-1)\sqrt{b(r-1)}, (2a-1)\sqrt{b(r-1)}, (2a-1)^2(r-1)), \\
 F_9 &= (-(2a-1)\sqrt{b(r-1)}, -(2a-1)\sqrt{b(r-1)}, (2a-1)^2(r-1)).
 \end{aligned}$$

Note that the first three fixed points are those of the uncoupled Lorenz system. To find out about the stability of these fixed points we need to calculate the eigenvalues of the corresponding Jacobian, J' . The partially block-diagonal form of the matrix makes the calculation easy:

$$J' = \begin{vmatrix} J & 0_{3 \times 3} & 0_{3 \times 2} \\ 0_{3 \times 3} & J & 0_{3 \times 2} \\ A & B & J_R \end{vmatrix}, \quad (5.6)$$

where, J is the Jacobian (eqn. 4) of the unperturbed Lorenz system of equations, $0_{m \times n}$ is a null matrix having m rows and n columns, and the other matrices are defined as,

$$A = \begin{vmatrix} 0 & a\sigma & 0 \\ 0 & a x_{f_3} & 0 \end{vmatrix}, \quad (5.7)$$

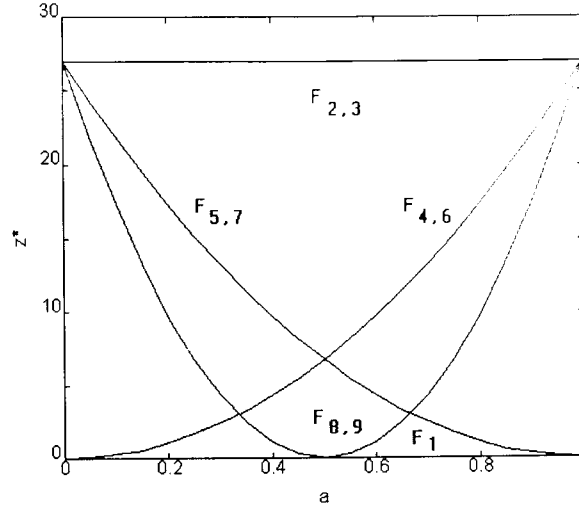


Figure 5.7: The z -coordinate of fixed points of the response system for $0 \leq a \leq 1$.

$$B = \begin{vmatrix} 0 & (1-a)\sigma & 0 \\ 0 & (1-a)x_{f_3} & 0 \end{vmatrix}, \quad (5.8)$$

and,

$$J_R = \begin{vmatrix} -\sigma & 0 \\ a y_{f_1} + (1-a)y_{f_2} & -b \end{vmatrix}. \quad (5.9)$$

Here f_k refers to the fixed point of the k th Lorenz system.

For $0 < r < 1$, the only stable fixed point is F_1 . For $r > 1$, F_1 loses its stability, and there are four new stable fixed points: F_2, F_3, F_8 and F_9 . For $r > r_c = \sigma(\sigma + b + 3)/(\sigma - b - 1)$, these fixed points lose their stability and the system shows only chaotic behavior. The most interesting instance is that of $a = 0.5$, where maximal competition occurs. In this case, $F_8 = F_9 = F_1$, $F_4 = F_5$ and $F_6 = F_7$ (Fig. 5.7). The attractor of the responding system is found to be stretched over its 3-dimensional phase space showing an extremely tangled structure (Fig. 5.6 (b)). This is due to the extremely complicated motion of the response system trajectory along the stable and unstable manifolds of the fixed points F_1, F_2, F_3, F_4 and F_6 . The coupling with driver system 1 tries to force the response system into synchronization with it, but at the same time, the coupling with driver system 2 desynchronizes the trajectory. The synchronization is therefore ‘frustrated’ by the competition between the two driver systems. The “frustrated” response system attractor reduces to the conventional Lorenz attractor if $a \rightarrow 0$ or 1, when competition is absent.

The attractor structure is found to be quite robust. If we start from two different initial conditions for the responding system, (x, y, z) and (x', y', z') , say, then for stable synchronization, the two respective trajectories should converge rapidly. However, whereas in the Pecora-Carroll case, convergence occurs to the standard Lorenz attractor, in this case, both the trajectories converge to the “frustrated” attractor.

The stability of synchronization can be demonstrated analytically by linear stability analysis of the error dynamics. Defining the dynamical error between two response system trajectories (\mathbf{x} and \mathbf{x}') which have different initial conditions, as $\mathbf{e} = \mathbf{x} - \mathbf{x}'$, the error equations can be written as:

$$\frac{de_x}{dt} = -\sigma e_x, \quad (5.10)$$

$$e_y = 0, \quad (5.11)$$

$$\frac{de_z}{dt} = (ay_1 + (1-a)y_2)e_x - be_z. \quad (5.12)$$

Here we have assumed that the equation parameters for the two systems are identical. The error system of equations has an equilibrium point at $\mathbf{e} = (0, 0, 0)$, which corresponds to perfect synchronization. The local stability of synchronization can then be checked by looking at the eigenvalues of the Jacobian of the error equations:

$$J_R = \begin{vmatrix} -\sigma & 0 \\ a y_1 + (1-a)y_2 & -b \end{vmatrix} \quad (5.13)$$

The eigenvalues are $-\sigma$ and $-b$, which are the conditional Lyapunov exponents of the response system. As both eigenvalues are negative, the synchronization is locally stable, and any difference in initial conditions rapidly goes to zero. Note that, this does not prove the global stability of the synchronized state. However, simulations have verified that even in the presence of large deviations in initial conditions, synchronization with the “frustrated” trajectory is achieved. This indicates that, although exact synchronization with the driver system cannot be achieved, the “frustrated” system can still be used for secure communication through chaotic masking. This has been established through simulations reported below.

Case II: $r_1 \neq r_2$

When the value of the r -parameter of the two driving systems is not the same, the fixed points are given by:

$$F_1 = (0, 0, 0),$$

$$F_2 = (a\sqrt{b(r_1-1)} + (1-a)\sqrt{b(r_2-1)}, a\sqrt{b(r_1-1)} + (1-a)\sqrt{b(r_2-1)}, a^2(r_1-1) + (1-a)^2(r_2-1) + 2a(1-a)\sqrt{(r_1-1)(r_2-1)}),$$

$$F_3 = (-a\sqrt{b(r_1-1)} - (1-a)\sqrt{b(r_2-1)}, -a\sqrt{b(r_1-1)} - (1-a)\sqrt{b(r_2-1)}, a^2(r_1-1) + (1-a)^2(r_2-1) + 2a(1-a)\sqrt{(r_1-1)(r_2-1)}),$$

$$F_4 = (a\sqrt{b(r_1-1)}, a\sqrt{b(r_1-1)}, a^2(r_1-1)),$$

$$F_5 = ((1-a)\sqrt{b(r_2-1)}, (1-a)\sqrt{b(r_2-1)}, (1-a)^2(r_2-1)),$$

$$F_6 = (-a\sqrt{b(r_1-1)}, -a\sqrt{b(r_1-1)}, a^2(r_1-1)),$$

$$F_7 = (-(1-a)\sqrt{b(r_2-1)}, -(1-a)\sqrt{b(r_2-1)}, (1-a)^2(r_2-1)),$$

$$F_8 = (a\sqrt{b(r_1-1)} - (1-a)\sqrt{b(r_2-1)}, a\sqrt{b(r_1-1)} - (1-a)\sqrt{b(r_2-1)}, a^2(r_1-1) +$$

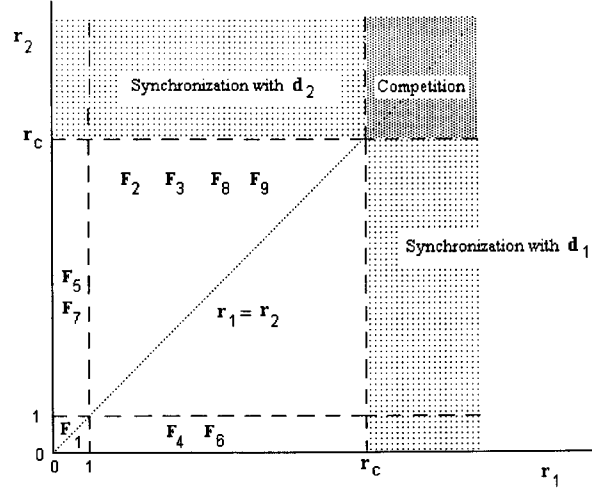


Figure 5.8: The (r_1, r_2) -parameter space showing the stable fixed points of the response system at different regions.

$$(1-a)^2(r_2-1) - 2a(1-a)\sqrt{(r_1-1)(r_2-1)}),$$

$$F_9 = (-a\sqrt{b(r_1-1)} + (1-a)\sqrt{b(r_2-1)}, -a\sqrt{b(r_1-1)} + (1-a)\sqrt{b(r_2-1)}, a^2(r_1-1) + (1-a)^2(r_2-1) - 2a(1-a)\sqrt{(r_1-1)(r_2-1)}).$$

Fig. 5.8 shows the (r_1, r_2) -parameter space. The stable fixed points at different regions are indicated in the diagram. The dotted line corresponds to the special case $r_1 = r_2$ which has been considered above. Note that, whereas in the general case all the fixed points are stable in some region or other, in the special case of $r_1 = r_2$, four of the fixed points, *viz.*, F_4, F_5, F_6 and F_7 , are always unstable. When one of the r -values go over to the chaotic regime, while the other r -value remains fairly below it, asymptotic synchronization with the chaotic trajectory is observed [106]. The time required to ultimately synchronize with the chaotic attractor is a function of both the r -parameter values. The synchronization is phase- synchronization rather than state- synchronization, as the response system chaotic attractor is a scaled replica of the driver system attractor. The scaling factor is a for synchronization with driving system 1, and $(1-a)$, for driving system 2. When both the r -values are in the chaotic regime, the “frustrated synchronization” situation occurs.

5.4 Simulation results

For conducting simulations, the parameter values chosen were $r_1 = r_2 = 28$, $\sigma = 10$ and $b = 8/3$. The trace of the Jacobian (which is equal to the sum of the Lyapunov exponents) for the total system, including the driver and response systems, is

-40.0. So the overall system is diffusive and possesses an attractor. The competition parameter a was varied in the interval $[0, 1]$. The differential equations were numerically solved using the fourth-order Runge-Kutta method with step-size = 0.025. The phase-space trajectory of the responding system (x_3, y_3, z_3) was observed with different values of a from $t = 0$ to $t = 100$. At the limit $a = 0$ (or 1) the responding system trajectory is identical to that of an unperturbed Lorenz system (Fig. 5.6 (a)). However, as $a \rightarrow 0.5$ (where maximal competition occurs), the trajectory deviates more and more from the standard Lorenz form. At $a = 0.5$, the trajectory moves in a complicated path around the fixed points F_1 , F_2 and F_3 (note that, at $a = 0.5$, $F_8 = F_9 = F_1$ (Fig. 5.6 (b))). It appears that for $a=0.5$, the z -variable time-series is much more correlated. This becomes clearer on taking a Fourier transform of the data. The power spectral density of the frustrated attractor time-series is low in the high-frequency end compared to the unperturbed system time-series.

The Lyapunov exponents were calculated using Gram-Schmidt technique [160] to create an orthonormal basis every 0.5 seconds of simulation time (this time interval being roughly half the “period” of the Lorenz system) and then averaging over 100 iterations. As expected, of the eight exponents, six correspond to those for the two unperturbed driving Lorenz systems (0.84, 0, -14.51). The remaining two exponents are the conditional Lyapunov exponents of the responding system : -8/3 and -10. This implies the robustness of the “frustrated” attractor - as any deviation from the attractor rapidly diminishes.

To study the degree of synchronization, z -coordinates of the responding system state (z_3) were plotted against the z -coordinates of each of the driver system states (z_1, z_2), for different values of a . If the two are synchronized, the plot gives a straight line. This suggests that the linear correlation coefficients, r , between the driver and response system time series, can be used to obtain a quantitative measure of synchronization. The linear correlation coefficient between two time series data $x(t)$ and $y(t)$ ($t = 1, \dots, n$), is given by

$$r_{x,y} = \frac{1}{n} \frac{\sum_{i=1}^n (x(i) - \bar{x})(y(i) - \bar{y})}{\sigma_x \sigma_y},$$

where \bar{x} and σ_x are the mean and standard deviation respectively, for the time series $x(t)$. A measure of desynchronization is defined as

$$\delta = 1 - r_{z_2, z_3}. \quad (5.14)$$

At $a=0$, where there is exact synchronization between driver system 2 and the response system, $\delta = 0$. This is a particularly robust measure, as $\delta \rightarrow 0$ for both state- and phase- synchronization. The variation of δ with a is shown in a logarithmic plot (Fig. 5.9). The linear nature of the curve over at least 3 orders of magnitude as $a \rightarrow 0$, indicates the presence of a power-law scaling relation of the form:

$$\delta \sim a^\beta, \quad (5.15)$$

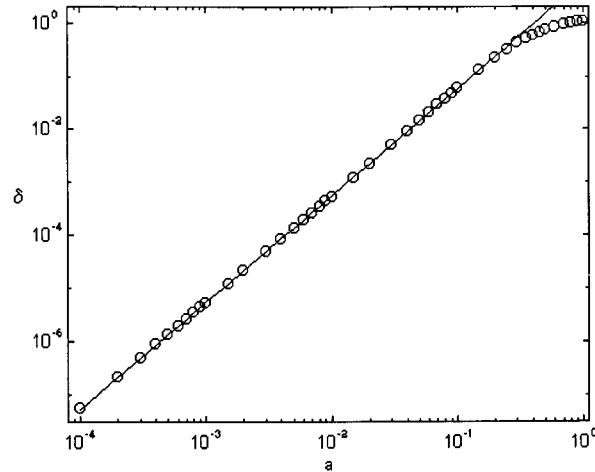


Figure 5.9: Log-scale plot of desynchronization (δ) for $0 < a \leq 1$. The power-law scaling relation (with characteristic exponent, $\beta \sim 2.0$) is indicated by the solid line fitted to the simulation data.

where the scaling exponent, $\beta \simeq 2.0$. The scaling exponent was also obtained for $r=50$ and 70 . In both cases, $\beta \simeq 2.0$ within simulation error. The scaling seems to be related to similar scaling phenomena due to intermittency induced by noise (in this case, the non-synchronized chaotic input) for motion on the invariant synchronization manifold [146, 136], that have been observed both theoretically [12, 83, 147, 45] and experimentally [207].

Another interesting feature studied was the fractal correlation dimension of the frustrated attractor (Fig. 5.10), calculated using the FD3 (ver. 0.3) software [154]. For the unperturbed Lorenz system, this is very close to 2, as the attractor is almost 2-dimensional. As a increases from 0 to 0.5, the attractor deviates from this two-dimensional shape, which can be quantitatively measured by the correlation dimension. As $a \rightarrow 0.5$, the attractor structure stretches out more and more over the three-dimensional space. This type of enhanced diffusion in phase space seems to be a generic feature of frustration in chaotic systems, and has been reported previously in the case of Coupled Map Lattices [20].

The simulations also showed the robustness of the “frustrated” attractor. Starting from different initial conditions, the response system trajectory was found to converge to the same attractor structure. This indicates that even in the absence of exact synchronization with any of the driver systems, the response system trajectory can be used as a chaotic masking signal for secure communication [42]. This was verified by adding a small amplitude periodic signal (e.g., a sine wave of frequency $\omega = 1/200$) to the response system y -variable time series. The resultant time series appears to be devoid of any periodic component (Fig. 5.11, top). It is then used to drive another

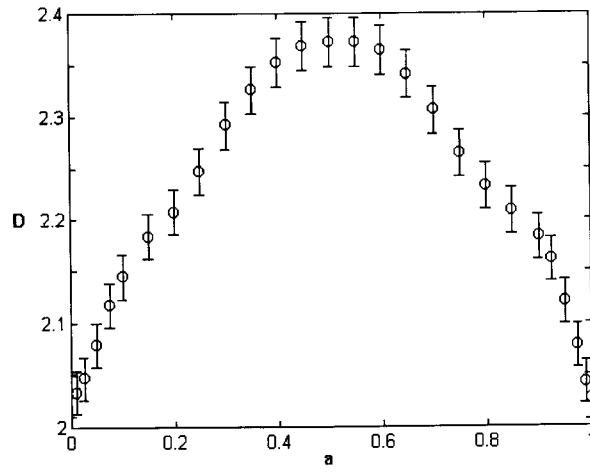


Figure 5.10: Correlation dimension of the response system attractor for $0 \leq a \leq 1$. The error is less than $\pm 10\%$.

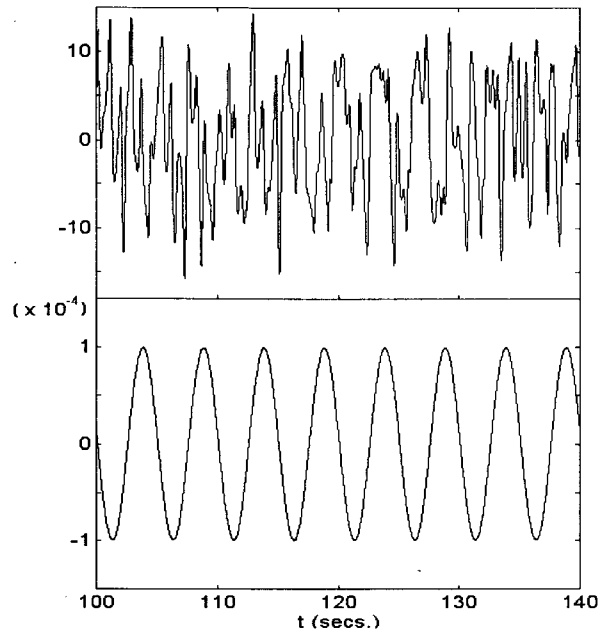


Figure 5.11: Chaotic masking: the x -variable time series of response system (top); the periodic signal obtained by subtracting the regenerated time series from the chaotic carrier wave (bottom).

Lorenz system, and the x -variable time series of the two systems are subtracted from each other to retrieve the original signal (Fig. 5.11, bottom). The modulation of the competition parameter, a , by a binary signal for chaotic switching, is another possibility of using the competitive scheme for secure communication.

5.5 Discussion

The competitive scheme described here for y -variable coupling was also implemented for x - and z -coupling of Lorenz systems. In the former, similar generalized attractor structure was observed, while in the latter, where the Pecora-Carroll synchronization does not work, no such structure could be observed. The work done here on coupled Lorenz systems can be extended to other systems defined by autonomous set of differential equations as well as discrete maps. However, it might be interesting to consider the result of competition in synchronizing non-autonomous systems (e.g., the Duffing oscillator). As such systems already have a forcing term present, which brings about the onset of chaos, the introduction of additional forcing terms can lead to qualitatively new behavior.

Competitive synchronization in extended systems might also lead to interesting phenomena. Lattices of (globally or diffusively) coupled chaotic elements, where each element can be used both to drive other elements, as well as respond to driving signals from yet another set of elements, and hence by a series of feedbacks drive its own driving systems, will serve to illustrate interactions between multiple competing synchronizing feedback loops. The motivation for such a study is that, in the human brain, synchronization of activity among different neurons appear to have an important functional role in the proper performance of perceptual tasks. It is to be noted that, single neurons are capable of chaotic behavior. As the brain is composed of densely connected networks of neurons, there is bound to be competitive synchronizing interactions between neural assemblies [193, 176]. A dynamic competition parameter, which causes synchronization-desynchronization transitions between various neural sub-assemblies, is a possible mechanism for information processing in biological systems. The resultant dynamics will be radically different from the one we are led to expect by observing the dynamics of single neurons or small groups of neurons.

The above work describes the simplest competitive scenario which can show a qualitatively different dynamics from that in the non-competitive situation. It is at present not known how the nature of synchronization and the attractor structure of the responding system might be altered by increasing the number of competing driver systems. In the brain, where each neuron is connected to $\sim 10^4$ other neurons, the competitive situation is bound to be far more complicated. The manner in which such an extremely competitive synchronization scenario might influence the way in which neural networks perform computations and process information is a very interesting problem for the future.